JOC The Journal of Organic Chemistry

Article

Thermal- and pH-Dependent Size Variable Radical Nano-particles and Its Water Proton Relaxivity for Metal-free MRI Functional Contrast Agents

Kosuke Morishita, Shuhei Murayama, Takeru Araki, Ichio Aoki, and Satoru Karasawa

J. Org. Chem., **Just Accepted Manuscript** • DOI: 10.1021/acs.joc.6b01509 • Publication Date (Web): 19 Aug 2016

ACS Publications

The Journal of Organic Chemistry is published by the American Chemical Society.
1155 Sixteenth Street N.W., Washington, DC 20036

Thermal- and pH-Dependent Size Variable Radical Nano-particles and Its Water Proton Relaxivity for Metal-free MRI Functional Contrast Agents.

Kosuke Morishita,[1] *Shuhei, Murayama,*[3] *Takeru Araki,*[1] *Ichio Aoki,*[3] *and Satoru Karasawa*[1,2]*

[1] Graduate School of Pharmaceutical Sciences, Kyushu University, 3-1-1 Maidashi, Higashi-Ku, Fukuoka, 812-8582 Japan. [2] PRESTO, Japan Science and Technology Agency, Kawaguchi, 332-0012 Japan. [3] Department of Molecular Imaging and Theranostics, National Institute of Radiological Sciences (NIRS), QST, Anagawa 4-9-1, Inage, Chiba-city, 263-8555 Japan.

Corresponding author: Satoru Karasawa.

E-mail: karasawa@phar.kyushu-u.ac.jp

TEL: +81-92-642-6593, FAX: +81-92-642-6545

ABSTRACT

For development of the metal-free MRI contrast agents, we prepared the supra-molecular organic radical, **TEMPO-UBD**, carrying TEMPO radical, as well as the urea, alkyl group, and phenyl ring, which demonstrate self-assembly behaviors using noncovalent bonds in an aqueous solution. In addition, **TEMPO-UBD** has the tertiary amine and the oligoethyleneglycol chains (OEGs) for the function of pH and thermal responsiveness. By DLS and TEM imaging, the resulting self-assembly was seen to form the spherical nano-particles 10 – 150 nm in size. On heating, interestingly, the nano-particles showed a lower critical solution temperature (LCST) behavior having two-step variation. This double-LCST behavior is the first such example among the supra-molecules. To evaluate of

the ability as MRI contrast agents, the values of proton (^{1}H) longitudinal relaxivity (r_1) were determined using MRI apparatus. In conditions below and above CAC at pH 7.0, the distinguishable r_1 values were estimated to be 0.17 and 0.21 $mM^{-1}s^{1}$, indicating the suppression of fast tumbling motion of TEMPO moiety in a nano-particle. Furthermore, r_1 values became larger in the order of pH 7.0 > 9.0 > 5.0. Those thermal and pH dependencies indicated the possibility of metal-fee MRI functional contrast agents in the future.

INTRODUCTION

Magnetic resonance imaging (MRI) is widely used as a non-invasive diagnostic method because of its properties of safety and deep penetration into the body. [1] To obtain bio-images emphasizing for the specific tissues such as a tumor tissue, contrast agents (CAs) are often used. Currently, Gadolinium (Gd) complexes are widely used as CAs because Gd ions have a largest spin quantum number of all the elements.[2] However, Gd complex CAs have potential side-effects such as renal disorder[3] due to the free Gd ion and a lack of specificity to the tissues. In addition, recently, accumulation in the brain, especially among children, was reported,[4] so the replacement of Gd complexes by new CAs is strongly desired. Stable organic radicals such as TEMPO are widely used as probes for bio-ESR imaging,[5] spin-trap against reactive oxygen species (ROS),[6] and so on. Such organic radicals can function as MRI CAs due to their possession of electron spin. However, their water proton relaxivity values (r_1 and r_2) are considerably smaller than those of Gd complexes.[7] To increase the relaxivity value, taking advantage of the suppression of fast tumbling of the TEMPO moiety rotational correlation time (τ_R) by enlarging the molecular size is a promising approach studied by many groups.[8] We previously reported that nano-particles with ~ 10 nm size consisting of amphiphilic oligonucleotides carrying TEMPO exhibited unexpectedly large r_1 value comparable with Gd complexes.[9] The resulting behavior was based on a slower molecular motion of the nano-particles and effective assembly of the water molecules against TEMPO

moiety. The exhibited high relaxivity indicated that using CAs with radicals is promising method for development of metal free CAs.[10] Separately, we reported that water-soluble supra-molecules consisting of urea benzene frameworks (UBDs) having oligoethyleneglycol chains (OEGs) showed thermal responsiveness in water solution (Figure 1).[11] Upon heating the solution, an abrupt self-assemble behavior with low temperature critical temperature (LCST)[12] took place due to the dehydration surrounding OEGs, to form micro-size particles. This LCST property is rare for supra-molecules.[13] This time, UBDs carrying TEMPO (**TEMPO-UBD**) as well as tertiary amino groups were prepared and thermal responsive behaviors accompanied by LCST and structural changes in solution were revealed. Furthermore, to confirm the driving force of the self-assembly of UBDs in water solution, UBD without TEMPO (**H-UBD**) as a hydrophobic moiety was prepared as reference compound and carefully compared to **TEMPO-UBD**. Using **TEMPO-UBD**, the water proton relaxivity values, r_1 and r_2, were determined under the conditions between pH 5.0 – 9.0. We herein describe the variations of physical properties and morphologies in response to various stimuli and evaluate the candidacy for metal-free MRI functional CAs. The molecular structures of **Tri-**, **H-** and **TEMPO-UBD** are shown in Figure 1.

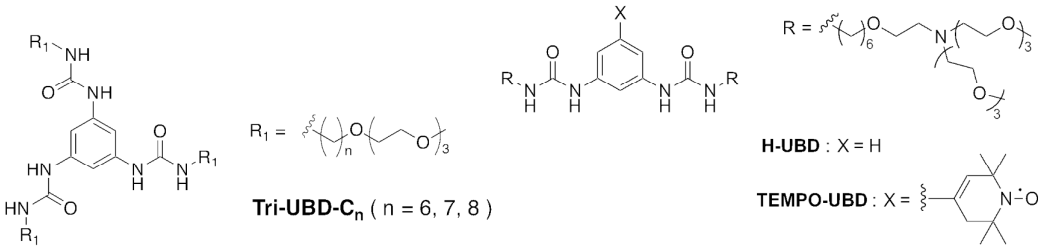

Figure 1. Molecular structures of **Tri-**, **H-** and **TEMPO-UBD**.

RESULTS and DISCUSSION

A. Syntheses of H- and TEMPO-UBD (Scheme 1).

A primary amine analogue having an amphiphilic side chain (**$Eg_3NEg_3C_6NH_2$**)[14] was

synthesized by three steps from 2-aminoethanol as the starting materials *via* a tertiary amine having bistriethyleneglycol at the amino group (**TEG_2EA**), an amphiphilic compounds (**$Eg_3NEg_3C_6Br$**), and a phtalimide having the amphiphilic chain (**$Eg_3NEg3C6Pht$**). The resulting **$Eg_3NEg_3C_6NH_2$** was coupled with 1-iodo-3,5-diisocyanatobenzene, to afford the diurea derivative having the amphiphilic chain (**Iodo-UBD**) as a colorless oil. The radical analogue having the amphiphilic chain (**TEMPO-UBD**) was prepared by Suzuki-Miyaura coupling[15] between **Iodo-UBD** and the TEMPO analogue having the boronic acid pinacolato ester.[16] The analogue **H-UBD** without TEMPO radical as the reference compound was prepared in a manner similar to **TEMPO-UBD** but using isophthalic acid in place of 5-iodoisophthalic acid. The synthesis routes of **H-** and **TEMPO-UBD** are shown in Scheme 1.

Scheme 1. Synthesis routes of **H-** and **TEMPO-UBD**.

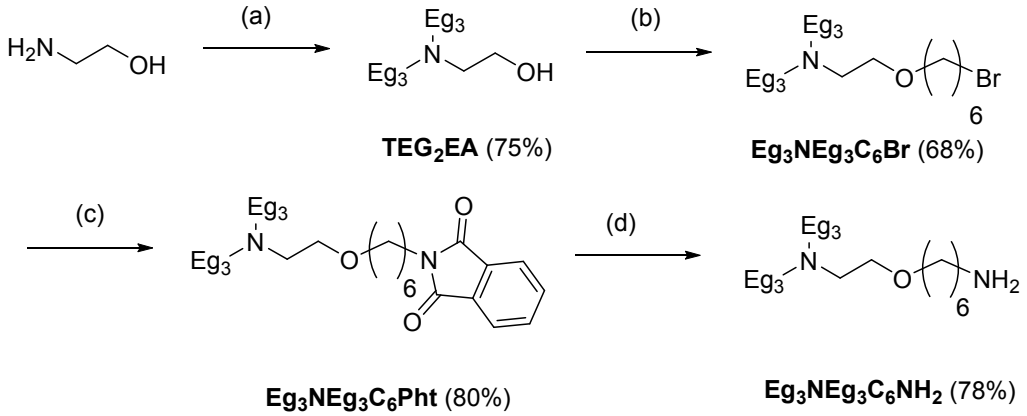

(a) Eg_3-Ts, K_2CO_3, MeCN, reflux; (b) 1,6-dibromohexane, NaH, THF, 0 ^oC;
(c) potassium phthalimide, DMF, 110 ^oC; (d) Hydrazine monohydrate, EtOH, reflux.

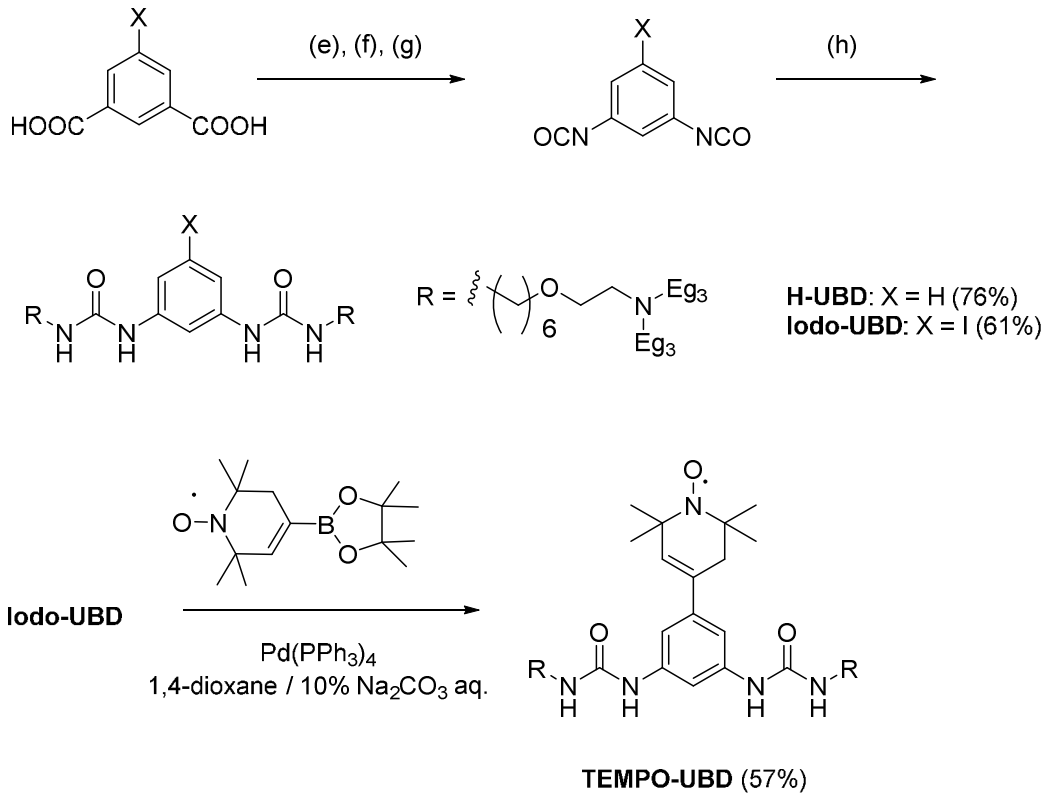

(e) $SOCl_2$, reflux; (f) NaN_3, THF/H_2O, 0 °C; (g) toluene, 100 °C;
(h) $Eg_3NEg_3C_6NH_2$, CH_2Cl_2 / toluene, 0 °C.

B. Self-assembly behaviors of H- and TEMPO-UBD in aqueous solutions.

To reveal the self-assembly behavior of **H-** and **TEMPO-UBD** in aqueous solutions, the concentration and the pH dependence of ^{1}H-NMR for **H-UBD** and ESR for **TEMPO-UBD** were examined using 0.1 – 10 mM solution at pH 9.0, 7.0, and 5.0 at 23 ºC.

B-1. ^{1}H-NMR of H-UBD in a buffer solution.

Before investigation of the self-assembly behavior, to determine the *pK*a value for **H-UBD**, pH titration of the chemical shift was performed (Figure S15 in S10).[17, 18] As the pH value decreased, the protons neighboring the N atom in the tertiary amino moiety were shifted downfield due to the protonation of amines.[19] The variation of the proton close to the N atom (H_g in Figure S15 in S10) was plotted with pH (Figure S16 in S11) and the *pK*a value of **H-UBD** was determined to be 7.6 according to eq. S1 in SI. This value indicates that the

protonation of amines took place completely and partially at pH 5.0 and 7.0, respectively, but not at all at pH 9.0. **TEMPO-UBD** having the same framework as **H-UBD** may be expected to show a similar *pK*a value.

(a)

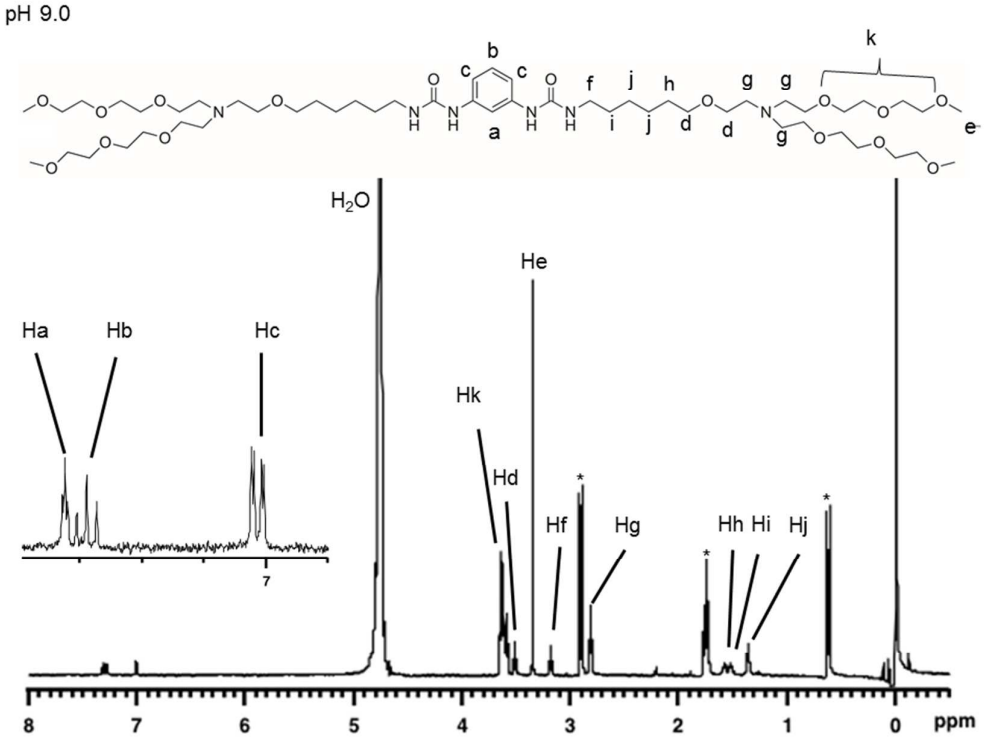

(b)

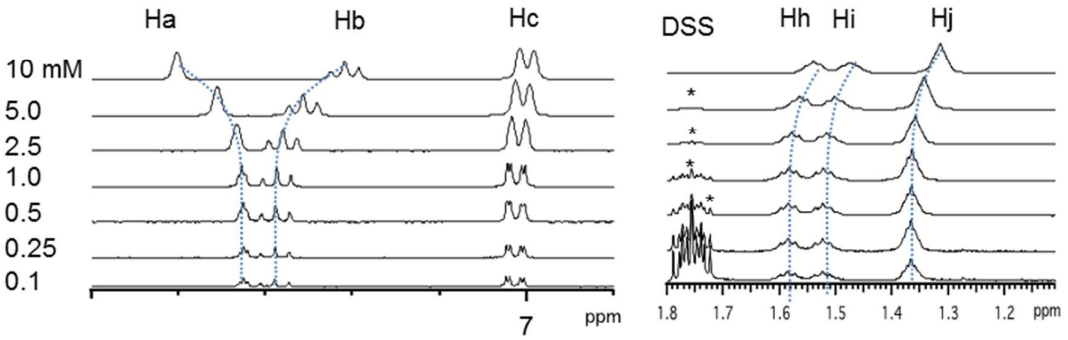

Figure 2. (a) ^{1}H-NMR spectra of **H-UBD** in 0.1 mM buffer solution at pH 9.0. (b) Concentration dependence of **H-UBD** in buffer solution at pH 9.0 in the expansions of aromatic (left) and alkyl chain (right) regions. Hxs indicate the protons corresponding the

molecular structure of **H-UBD** (upper). The dotted blue lines represent the fitting curves according to the isodesmic model (See text). The asterisks denote the proton of DDS as standard material.

In the lowest concentration of 0.1 mM buffer solution at pH 9.0, protons corresponding to the benzene ring (H_a, H_b, and H_c), oligoethyleneglycol chains (OEGs)(H_d, H_e, H_g, and H_k) and the alkyl chains (H_f, H_h, H_i, and H_j) were observed at 7.3 - 7.0, 3.7 – 2.8, and 3.2 – 1.3 ppm, respectively (Figure 2a). As the concentration increased from 0.1 to 10 mM (Figure 2b), the protons at the aromatic region (H_a and H_b), neighboring a tertiary nitrogen (H_g), and alkyl chains ($H_{h\text{-}j}$) clearly shifted with the broadening. In contrast, the peaks corresponding to the OEGs showed little shifting. The observed upfield shifts of H_b, H_g, and $H_{h\text{-}j}$ indicate the typical behaviors of formation of the aggregate due to the shielding effect among the molecules.[20] In contrast, a downfield shift was observed in H_a, which is the proton in ortho position of two urea groups, revealing the formation of a pseudo-hydrogen bond between H_a and O atoms in the carbonyl group of urea moiety (Figure S19(b) in S14).[21] This interaction might be led by the formation of the aggregate, and a similar deshielding of proton was observed in the analogue of **Tri-UBD**, as previously reported.[11]

(a)

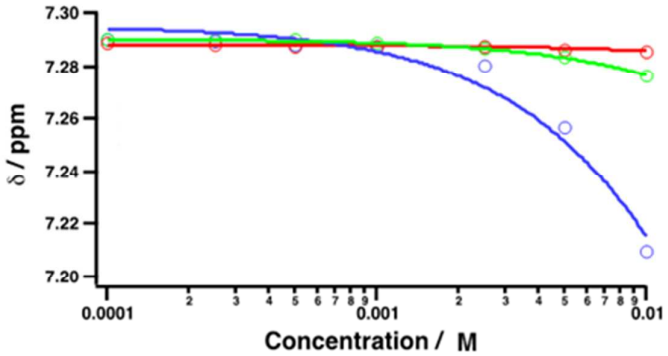

(b)

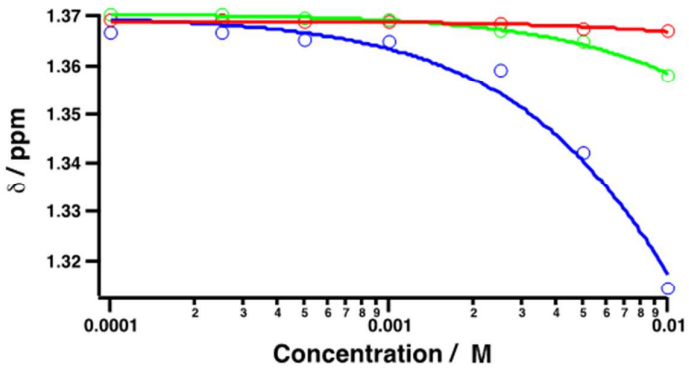

Figure 3. Plots of chemical shifts of H_b (a) and H_j (b) *vs* concentration for **H-UBD** at pH 9.0 (blue), 7.0 (green), and 5.0 (red). The solid lines indicate the theoretical curves according to the isodesmic model. See the text and Table 1.

The resulting chemical shifts of H_b, H_g, and H_j were plotted as functions of the concentration (Figures 3 and S19 (a)). To evaluate the aggregation behavior, the shifting peaks were fitted according to the isodesmic model (eq. S2 in S13),[22, 23] to give association constants (*K*) of 12.3 ± 0.1, 54.3 ± 11.8, and 16.2 ± 0.1 M^{-1} in H_b, H_g, and H_j, respectively (Table 1). Furthermore, the inflection points in the curvature suggested that the value of critical aggregation concentration (CAC) was 0.5 mM. Even though the concentration was over CAC and the aggregate was forming, the peaks corresponding to OEGs showed little shifting even at the highest concentration. This suggested that the OEGs were located outside the aggregate so the OEGs could move and/or rotate faster than the benzene ring and alkyl group. In neutral and acidic conditions at pH 7.0 and 5.0 of 0.1 mM, the obtained chemical shifts consisted of peaks at pH 9.0 except for H_g, which corresponded to the peak neighboring the tertiary N atoms (Figures S15 and S19(a) in S10 and S14). Deshielding shifts of H_g were observed in the order pH 9.0 < 7.0 < 5.0, suggesting that the protonation took place at N atoms. In the plot of chemical shift *vs* concentration, even though concentration dependences similar to those at pH 9.0 were observed, the degree of change in the chemical shifts was smaller than for those at

pH 9.0. The resulting *K* values in H_b, H_g, and, H_j, by fitting with the isodesmic model were 4.03 ± 0.01, 3.50 ± 0.01, and 4.31 ± 0.01 M^{-1} at pH 7.0 and 1.35 ± 0.01, 1.28 ± 0.01, and1.37 ± 0.25 M^{-1} at pH 5.0. Comparing to the *K* values between various pH conditions, the estimated *K* values increased in the order pH > 9.0 > 7.0 > 5.0 suggesting that protonated **H-UBD** in acidic conditions was suppressed to form the aggregates owing to Coulomb repulsion and/or increased hydrophilicity. The CAC values under conditions at pH 7.0 and 5.0 were 1 and 5 mM, respectively. The ^{1}H-NMR spectrum of **H-UBD** in 0.1 m M and the concentration dependence at pH 9.0 are shown in Figure 2 a) and b). Similar spectra at pH 7.0 and 5.0 are shown in Figure S17 (S12). The plots of H_b and H_j, and H_g as a function of concentration at pH 9.0, 7.0, and 5.0 with the fitting curves are shown in Figure 3 and Figure S19 (a) (S14). The obtained values of *K* and CAC are summarized in Table 1.

Table 1. Values of Association Constants (*K*) Estimated from Isodesmic Model and CAC under Various Concentrations at pH 9.0, 7.0, and 5.0.

pH	*K* values (M^{-1})			CAC (mM)
	H_a	H_g	H_j	
9.0	12.3 ± 0.1	54.3 ± 11.8	16.2 ± 0.1	0.5
7.0	4.03 ± 0.01	3.50 ± 0.01	4.31 ± 0.01	1
5.0	1.35 ± 0.01	1.28 ± 0.01	1.37 ± 0.25	5

B-2. EPR spectra of TEMPO-UBD in buffer solution.

X-band (ν_0 =9.4 GHz) ESR measurements at various concentrations (0.1 – 2.0 mM) were performed at pH 9.0, 7.0, and 5.0. In the lowest concentration of 0.1 mM **TEMPO-UBD** solution at pH 9.0, peaks with three well-resolved lines due to splitting of the nucleus spin of an N atom were observed at g = 2.0048 (Figure 4). The peak in the highest field showed the

weaker intensity and slight broadening compared to those typical TEMPO analogues, indicating that the slow rotational correlation time (τ_R) took place even at 0.1 mM due to the large molecular size of **TEMPO-UBD**. As the concentration increased, the peak in the highest field became slightly weaker, and broadened above 0.76 mM.

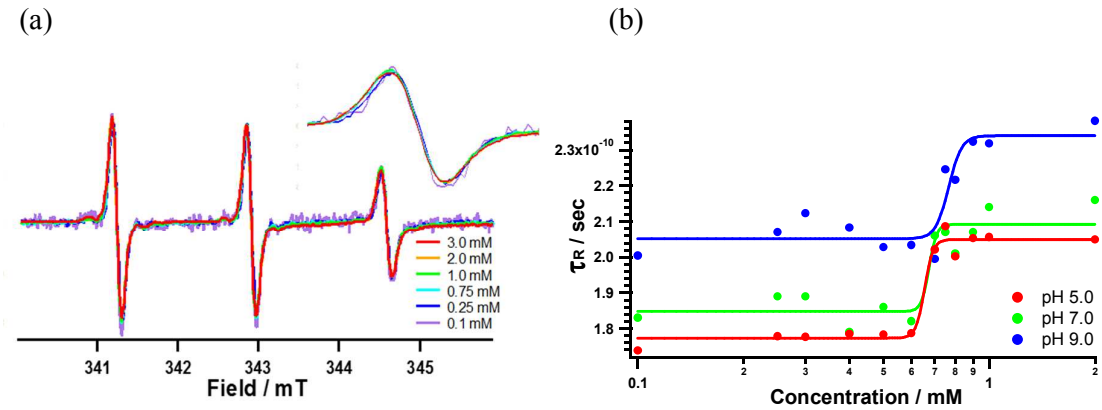

Figure 4. (a) Normalized ESR spectra of **TEMPO-UBD** in 2.0 – 0.1 mM buffer solutions at pH 9.0. Spectra were normalized by intensity at center peaks. Inset shows a magnified peaks at highest field. (b) Plots of τ_R values estimated by Kivelson's equation vs concentration at given pHs. The colored solid line indicate the sigmoidal fitting as a guide.

To evaluate the global motions of molecules and local motion of TEMPO moiety below and above 0.76 mM, τ_R values using Kivelson's equation[24] were estimated as 2.05 x 10^{-10} and 2.34 x 10^{-10} s, respectively (Figure 4, S20, and eq. S3 in S15). The resulting values above 0.76 mM were16 and 1.1 times larger than those of typical TEMPO (1.5 x 10^{-11} s) and the solution of **TEMPO-UBD** below 0.76 mM, suggesting the formation of aggregate as seen for **H-UBD**, and the inflection concentration implied the CAC value of **TEMPO-UBD** at pH 9.0. At pH 7.0 and 5.0, furthermore, the inflection points of τ_R values were both observed at the similar concentration of 0.66 mM. Even though similar CAC values between pH 9.0, 7.0, and 5.0 were observed, the estimated τ_R values showed a large difference. Below and above CAC at

pH 7.0, and 5.0, the τ_R values were 1.85 and 2.09 x 10^{-10} s, for pH 7.0 and 1.77 and 2.04 x 10^{-10} s for pH 5.0, respectively. Below and above CAC, the obtained τ_R values increased in the order pH 9.0 > 7.0 > 5.0. Below CAC, **TEMPO-UBD** in pH 5.0 solution exists as cationic monomer protonated at the tertiary N atoms, to give the fast molecular motion and smallest τ_R values due to Coulomb repulsion, while in pH 9.0 solution, the monomer of **TEMPO-UBD** exists as a neutral form and showed the largest τ_R values compared to those at pH 7.0 and 5.0. Above CAC, the resulting aggregate including Coulomb repulsion in an acidic condition also gave faster molecular motion and smaller τ_R values. In addition, the neutral aggregate gave the slower molecular motion and larger τ_R values. Comparing the CAC values estimated from ^{1}H-NMR for **H-UBD** and ESR for **TEMPO-UBD**, the values of **TEMPO-UBD** were smaller than those of **H-UBD**, indicating that the association constant (*K*) of **TEMPO-UBD** might be higher than that for **H-UBD**. The difference of the self-assembly behaviors among UBDs is responsible for the hydrophobicity of TEMPO moiety. ESR spectra of **TEMPO-UBD** in 2.0 – 0.1 mM buffer solutions at pH 9.0, 7.0, and 5.0 are shown in Figure 4(a) and S21(S15). Plots of τ_R *vs* concentration at pH 9.0, 7.0, and 5.0 are shown in Figure 4 (b). The τ_R values obtained under various conditions are summarized in Table 2.

Table 2. Values of τ_R (s) Estimated from Kivelson's Equation and CAC under Various Concentration Conditions at pH 9.0, 7.0, and 5.0.

pH	τ_R (10^{-10} s)		CAC (mM)
	Below CAC	Above CAC	
9.0	2.05	2.34	0.76
7.0	1.85	2.09	0.66
5.0	1.77	2.04	0.66

C. Thermal behaviors of H- and TEMPO-UBD in water and buffer solution.

C-1) Transmittance change of H- and TEMPO-UBDs by heating process.

We previously reported that the urea benzene derivatives (UBDs) carrying the OEGs showed thermal responsiveness in an aqueous solution, to give a cloudy solution with lower critical solution temperature (LCST) by heating.[11] This behavior is based on the dehydration surrounding OEGs in response to temperature, such that the self-assembly is accelerated by the increase of hydrophobicity of the molecules as well as the increasing size of the aggregate. To understand the thermal behavior of **H-** and **TEMPO-UBD**, the transmittance at 800 nm was monitored in the range 20 – 70 ºC at various pHs.

In the case of 5 mM **H-UBD** solution at pH 9.0, which is above CAC, the transparent solution turned abruptly cloudy at 48 ºC, which corresponds to the LCST value, and the resulting cloudy solution was maintained over 70 ºC (Figure 5(a)). In contrast, the solution at 0.1 mM, which is below CAC, showed no LCST behavior until 70 ºC, indicating a dependency on concentration. Similarly, the thermal behaviors in 5 mM buffer solution at various pH conditions were tested: LCST behavior at 63 ºC and no LCST behavior until 70 ºC, the same as for the dilute solution, were observed at pH 7.0 and 5.0, respectively. As the pH values decreased, the LCST became higher in the order pH 9.0 < 7.0 < 5.0, indicating that aggregates including the cation moiety in acidic conditions can't easily form a large size aggregate and/or the amount of the aggregate is maintained. This is because Coulomb repulsion between cationic species took place by itself and/or the cationic species showed a large hydrophilicity than under basic conditions.

In the case of **TEMPO-UBD** in phosphate buffer solutions, interestingly, two-step decreases of the transmittance were observed (Figure 5(b)). At pH 9.0, the first and second steps began at 31 and 37 ºC, respectively. The former step showed gradual change of the transmittance from 98 to 83%, and the latter step changed abruptly from 83 to 0%. Similar two-step LCST behaviors were observed at pH 8.0, and 7.0. This two-step behavior has been reported in the case of polymer compounds and was classified as "double –LCST behavior".[25] It was noted that this thermal double-LCST behavior is first such example among the supra-molecule

category. Furthermore, it was found that missing double-LCST behavior took place in the conditions using a pure water solution, and in the case of **H-UBD** even at a high concentration.

(a-1)

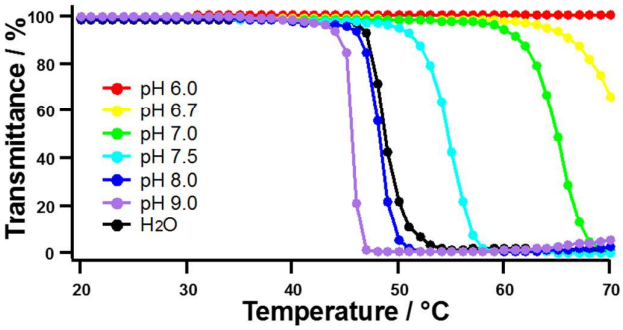

(a-2)

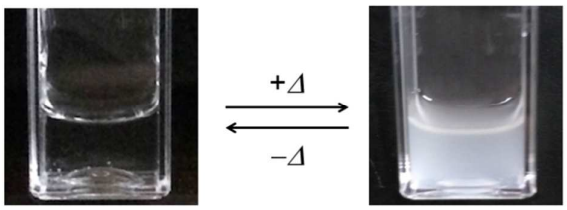

(b-1)

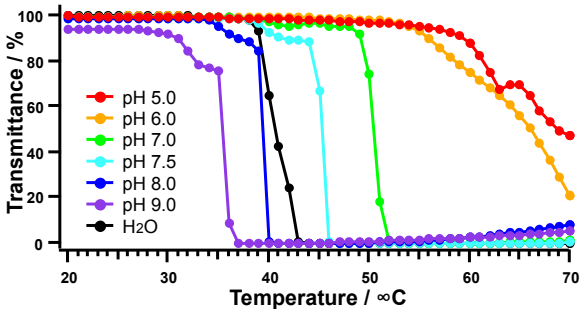

(b-2)

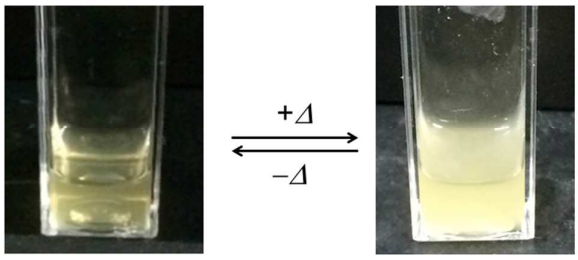

Figure 5. Thermal responsiveness monitored by changes of the transmittance at 800 nm in 5 mM aqueous solutions of (a) **H-UBD** and (b) **TEMPO-UBD** at given pHs and in pure water condition (black). The pictures indicate the change between transparent and turbid solutions in vials by thermal stimulus (5 mM at pH 7.0).

The abrupt decrease of the transmittance observed in the 2nd step corresponds to the typical LCST behavior due to self-assembly by the dehydration surrounding OEGs. The gradual decrease of the transmittance observed in the 1st step might be led by the demetalation and consequently the self-assembly process in buffer solution including the salts of NaCl and KCl. Above 50 ºC, in addition, a gradual increase of the transmittance occurred until 70 ºC, suggesting the formation of precipitation due to a stronger dehydration effect. Actually, small precipitations in a cuvette were observed during the measurement at 70 ºC. Comparing the LCST behavior between **H-** and **TEMPO- UBD**, the LCST value of **TEMPO-UBD** shifted to a lower temperature in same conditions, suggesting that the hydrophobicity in the aggregates consisting of **TEMPO- UBD** was higher than in those of **H-UBD**. The reason for no double-LCST behavior in the **H-UBD** might be the differences in hydrophobicity and stability for the aggregate in buffer solution. The thermal responsiveness monitored by changes of the transmittance at 800 nm in 5 mM aqueous solutions of **H-** and **TEMPO-UBD** at given pHs, in addition in a pure water are shown in Figure 5 and Figure S22 (S16). The thermal variation between transparent and turbid solutions into vials were photographed and are represented in Figure 5.

Table 3. LCST Values of **H-** and **TEMPO-UBD** under Various pH Conditions.

	LCST value (ºC)	
pH	**H-UBD**	**TEMPO-UBD**
9.0	45	31*
		37$^{\#}$

8.0	47	36*
		40#
7.0	63	42*
		51#
6.0	N. D.	56
5.0	-	64
Water	48	39

*and # indicate the values at starting the 1st and the 2nd LCST steps, respectively.

C-2. Variable Temperature DLS measurements of H- and TEMPO-UBD in a buffer solution.

To understand the size of aggregate as well as the thermal self-assembly accompanying LCST, variable temperature dynamic light scattering (VT-DLS) measurements in 5 mM of aqueous solutions were performed for **H-** and **TEMPO-UBD,** respectively. Each hydrodynamic diameter (D_H) was estimated as the average of three time measurements. The 5 mM solutions was selected as the concentration forms the aggregate in both **UBDs** derivatives.

In a buffer solution at pH 9.0 for **H-UBD** (Figure 6a), single broadening peaks corresponding to D_H values of 10~80 and over 1000 nm were observed at 20 and 58 ºC, respectively, indicating that the aggregate below LCST was nano-particles 10~80 nm in size and the grown aggregate above LCST was micro-particles over 1000 nm in size. In the neutral condition (Figure 6a), similar D_H values of 20~100 and ~1000 nm at pH 7.0 were observed below (20 ºC) and above LCST (70 ºC), indicating that nano-particles and micro-particles were formed below and above LCST. In addition, the pH dependence was negligible (Table 4). Even in pure water, the resulting D_H values were consistent with those in buffer solution (Figure S22 in S16). In contrast, in **TEMPO-UBD** with pH 9.0 solution (Figure 6b and c), which had the double-LCST behavior at 31 and 37 ºC (Figure 5 and Table 3), the D_H values at 24 and 36 ºC showed 30~150 nm as a single broadening peak, and two broadening peaks at

~300 and over 1000 nm, respectively, suggesting that nano-particles 30~150 nm in size, as for **H-UBD**, and grown particles over 100 nm in size were formed below and above the 1st LCST step. Above the 2nd LCST of 40 ºC, all particles exhibited over 1000 nm in size and the resulting thermal behavior was consistent with those of **H-UBD**.

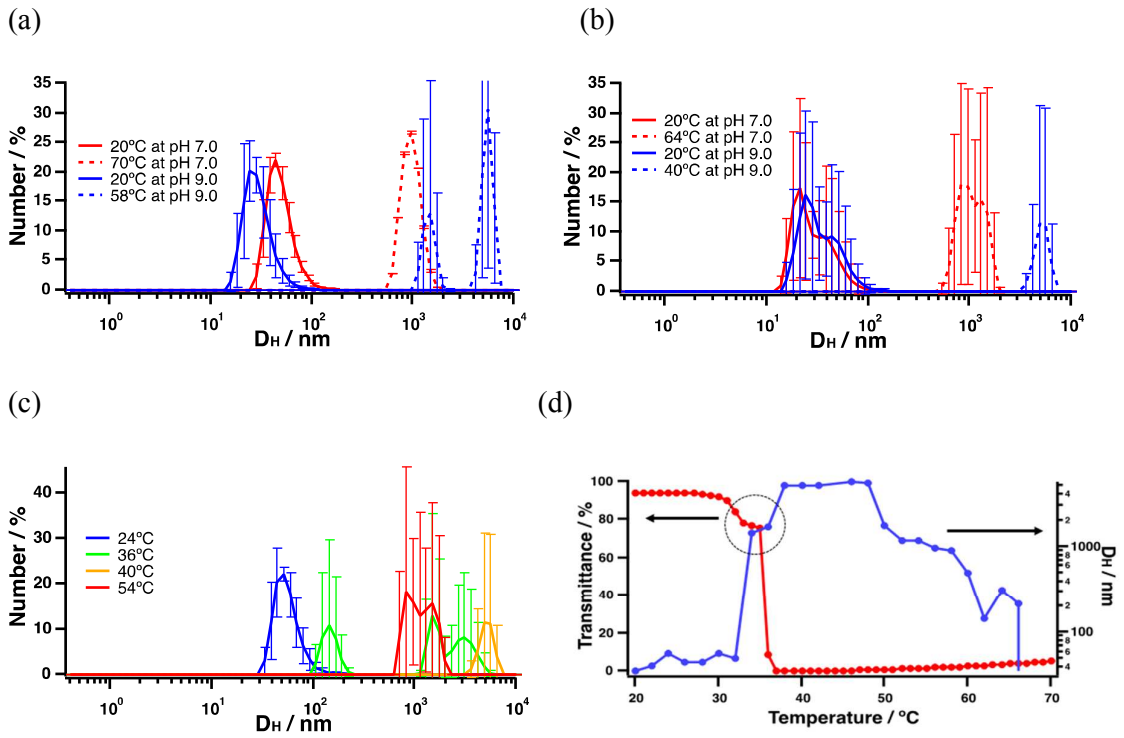

Figure 6. Variable temperature DLS measurement in 5 mM buffer solutions. D_H values of (a) **H-UBD** and (b) **TEMPO-UBD** for given conditions of temperatures and pHs. (c) Detailed changse of D_H values at various temperature at pH 9.0 for **TEMPO-UBD**. (d) Plots of the average D_H value (right axis and blue mark) and transmittance (left axis and red mark) change *vs* temperature at pH 9.0 for **TEMPO-UBD**. Dotted circle in (d) represents the steady step between the 1st and 2nd LCST behaviors.

To reveal the relationship between the transmittance and D_H value, the D_H values changed by the heating process were plotted as a function of the temperature accompanied by the

transmittance change (Figure 6d). As the temperature increased from 20 to 48 ºC, two non-continuous increase of D_H values were observed at 32 and 36 ºC, suggesting that changes in particle size took place at the same temperature as the double-LCST behavior obtained from the thermal transmittance change (left axis in Figure 6d). As the temperature increased above 48 ºC, a decrease of the micro-particle size was observed. This behavior occurred due to the formation of precipitations by a stronger dehydration effect (*vide supra*). At pH 7.0 and in pure water for **TEMPO-UBD** (Figures 6(b) and S23 in S17), comparable size changes with pH 9.0 were observed below and above LCST. Comparing the size of the particles between **H-** and **TEMPO-UBD**, even though **TEMPO-UBD** introduced a TEMPO moiety into **H-UBD**, no considerable difference in the particle size below and above LCST was seen. The obtained D_H values of **H-** and **TEMPO-UBD** under variable temperature and pH are shown in Figure 6a and b and are summarized in Table 4. The detailed changes of D_H values at various temperatures at pH 9.0 for **TEMPO-UBD** are shown in Figure 6c. Plots of D_H value (right axis) and transmittance (left axis) change *vs* temperature at pH 9.0 for **TEMPO-UBD** are given in Figure 6d.

Table 4. Temperature and pH Dependencies of the Size Obtained from DLS for **H-** and **TEMPO-UBD** with 5 mM Buffer Conditions.

Temperature ranges (ºC)	Size / nm (ºC)					
	H-UBD			**TEMPO-UBD**		
	pH 9.0	pH 7.0	Pure water	pH 9.0	pH 7.0	Pure water
20	10~80	20~100	7~60	10~150	10~150	20~150
21–30				30~150 (24)		
31 –40				100~ (36), 3000~ (40)		
41–50				~1000 (50)		
51 – 69	~1000 (58)			100 (60)	~1000 (68)	
70		~1000	~700			~1000

The parentheses indicate the temperature recorded DLS data.

C-3) TEM and SEM images of H- and TEMPO UBD.

To identify the morphologies of the solution samples, transmission electron microscopy (TEM) were carried out and stained images for **H-** and **TEMPO-UBD** were obtained. In addition, scanning electron microscopy (SEM) for **TEMPO-UBD** was performed. In TEM, the 5 mM water solution samples were mounted as 5 μl on a carbon grid with hydrophilic treatment and the residual solution was sucked up by a filter paper at 23 ºC for the sample below LCST. In contrast, the residual solution was evaporated at 70 ºC for the sample above LCST. Each sample was stained with 5% uranyl acetate solution for the negative stained images. The salts often prevented observation of the morphology for organic materials even after staining so the samples prepared in pure waters solution were used. In SEM, the samples were prepared from freezing-dry for the below LCST, while heated at 100 ºC on hot plate for the sample above LCST. Each sample was coated with Pt moisture on a carbon tape onto a stage.

c-3-1) TEM.

In **H-UBD**, spherical nano-particles 20 ~ 60 nm in size were obtained below LCST, while amorphous-like assembly of over 100 nm in size were observed in the samples above LCST (Figure 7a and S25 in S18). The sizes obtained below and above LCST were slightly smaller than those obtained from DLS measurements. This suggests that the samples in solution included water molecules, making the sizes of samples obtained by DLS larger size compared to those on TEM images. In the case of **TEMPO-UBD** (Figure 7b and S25 in S18), the sample below LCST showed spherical nano-particles with 10- 150 nm sizes same as **H-UBD**. In contrast, the samples above LCST exhibited formation of assemblies consisting of nano-particles of size 300- 500 nm. The resulting sizes below and above LCST were smaller than those estimated from DLS measurement for the same reason as with **H-UBD**. Above

LCST, interestingly, a distinguishable morphology difference between **H-** and **TEMPO-UBD**, being amorphous-like particles and assemblies of the nano-particles, was clearly observed.

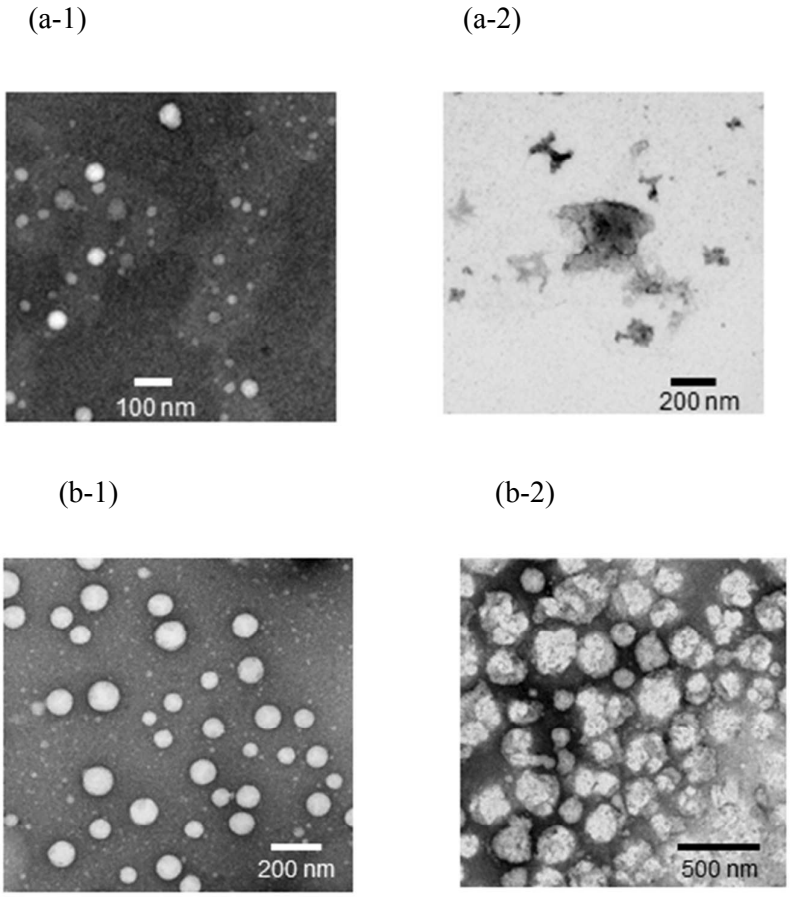

Figure 7. TEM images of (a) **H-** and (b) **TEMPO-UBD** prepared at (1) 23 and (2) 70 ºC. Scale bars indicate (a-1)100, (a-2) 200, (b-1) 200, and (b-2) 500 nm, respectively.

c-3-2) SEM.

In the sample after freezing-dry for **TEMPO-UBD**, many spherical nano-particle ~ 60 nm in size were clearly observed. In contrast, the image of sample heated at 100 ºC showed the grown particles with 100 ~ 500 nm in size and looks like the disordered amorphous shape, even though the TEM image gave the ordered assemblies consisting of nano-particles. This

discrepancy might resulted from melting of the particles on a hot plate under preparing the SEM sample. TEM mages and plots of count *vs* diameter for **H-** and **TEMPO-UBD** are shown in Figure 7 (a) and (b), and S25 (in S18). SEM images for **TEMPO-UBD** are shown in Figure S26 in S19.

C-4) Structured differences of self-assembly between H- and TEMPO-UBD.

Comparing the thermal properties and the morphologies between **H-** and **TEMPO-UBD**, interestingly, we observed distinguishable differences in the LCST behavior and the morphology above LCST were observed. With respect to the LCST behaviors, double-LCST behavior was observed only in the case of **TEMPO-UBD**. Furthermore, the morphology of the micro-particles obtained above LCST was different with micro-particle being disordered amorphous or ordered assemblies of nano-particles in **H-** and **TEMPO-UBD**, respectively. These results suggest that different thermal self-assembly behaviors took place by different mechanisms at the molecular level. Below LCST, the nano-particles of both **H-** and **TEMPO-UBD** were hydrated with many water molecules and metal ions at OEGs in the buffer solution. As the temperature increased, initially demetallation and then dehydration surrounding OEGs took place, creating more hydrophobicity at the molecule level and in grown micro-particles. In the case of the **H-UBD** sample (Figure 8a), upon heating the spherical nano-particles sized ~100 nm collapse and the resulting amorphous micro-particles might form a disordered random monomer. Although **UBDs** are supra-molecules, the micro-particles formed a globule-like structure, as also reported in thermo-responsive water-soluble polymers such as PNIPAM.[26] In the case of the **TEMPO-UBD** (Figure 8b), in contrast, the spherical nano-particles 20~ 150 nm in size obtained below LCST accumulated by themselves and maintained their morphology and size even at 70 ºC, to give new particles of micrometer order. Since the hydrophobicity of **TEMPO-UBD** is higher than that of **H-UBD**, the stability of the nano-particles composing **TEMPO-UBD** in aqueous solution is

also higher than that of **H-UBD**, so a difference in morphology change took place in both **UBDs** over LCST. With respect to the double-LCST behavior in **TEMPO-UBD**, we consider that the 1st and the 2nd steps of LCST correspond to the demetallation and dehydration processes, respectively (Figure 8b). Even though the conditions were similar, the absence of double-LCST behavior in **H-UBD** is likely to be led by the weaker association constant of the nano-particles and so disordered micro-particles (globules) were observed. The plausible structures and thermal mechanism of **H-** and **TEMPO-UBD** in buffer solution are shown in Figure 8.

(a)

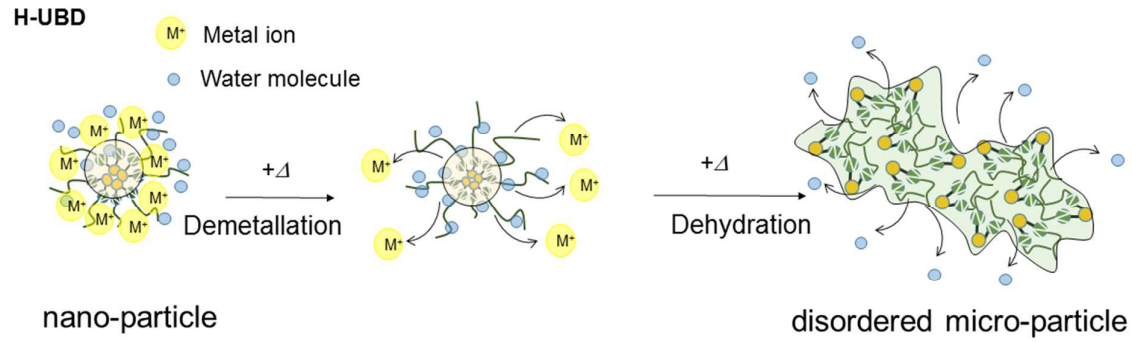

(b)

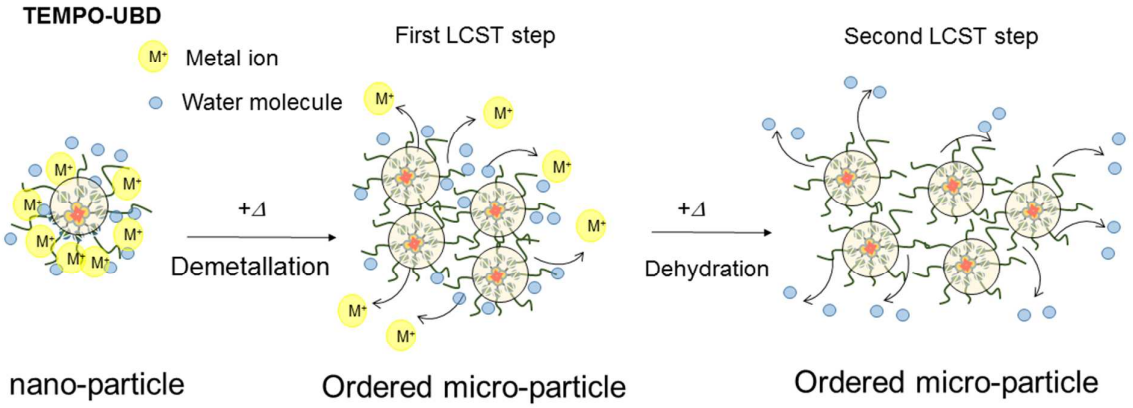

Figure 8. Schematic drawing of plausible structures of (a) **H-** and (b) **TEMPO-UBD** in buffer solution.

D) Water-proton longitudinal and transverse relaxivity (r_1 and r_2) and MR imaging of TEMPO-UBD in aqueous conditions at pH 9.0, 7.0, and 5.0.

To reveal the potential of **TEMPO-UBD** as a MRI contrast agent, water-proton relaxivites, r_1 and r_2, were determined from relaxation times, T_1 and T_2 obtained using 7 T MRI apparatus at various concentrations and at pH 9.0, 7.0, and 5.0, respectively. In addition, T_1- and T_2 –weighted images were acquired (Figure 10). Considering bio-imaging applications, the T_1 and T_2 values were obtained at 23 ºC maintained using a gradient coil cooling system and air conditioners. Samples at 10.0, 7.5, 5.0, 3.3, 2.5, 1.0, 0.5, 0.25, and 0.125 mM were prepared in PCR tubes and used. The values of r_1 and r_2 were estimated from the slopes in the plots of T_1^{-1} or T_2^{-1} *vs* concentration. To evaluate the r_1 and r_2 values of **TEMPO-UBD**, those values were compared with simple TEMPO derivatives of **Oxo-TEMPO**.

(a)

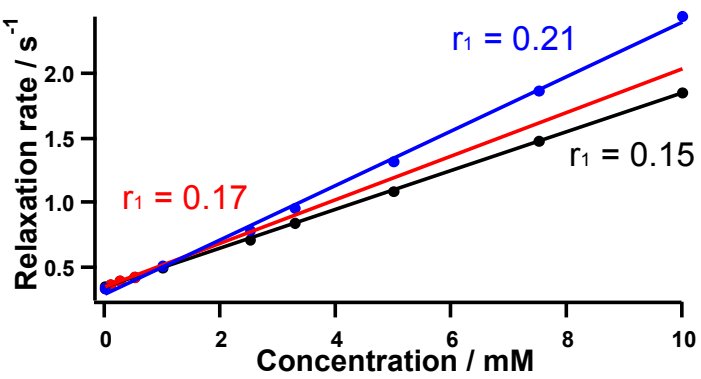

(b)

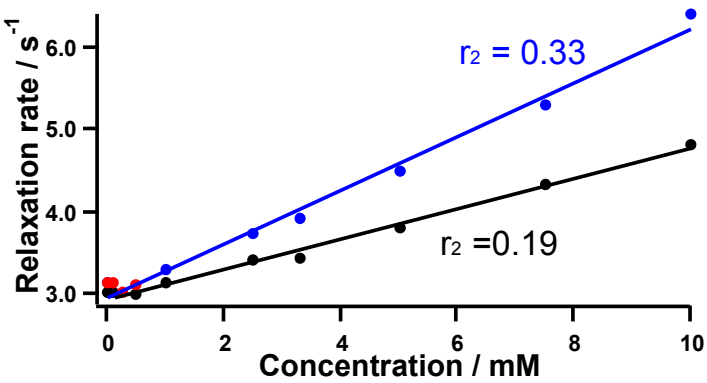

Figure 9. Plots of (a) T_1^{-1} and (b) T_2^{-1} *vs* concentration for **TEMPO-UBD** (blue and red) and **oxo-TEMPO** (black) as reference at pH 7.0. The ranges for higher (10.0 – 1.0 mM) and lower (0.5 – 0 mM) concentrations of **TEMPO-UBD** are shown blue and red filled circles, respectively. The solid lines indicate the least squares fitting of each slope.

The plots of relaxation rate, T_1^{-1} or T_2^{-1} at pH 7.0 *vs* concentration are shown in Figure 9. There were two different slopes, below and above 1.0 mM. From the τ_R value estimated from ESR at pH 9.0, nano-particles formed above CAC value of 0.76 mM, which is consistent with the inflection values of 1 mM of r_1 and r_2. The values below and above CAC of r_1 were 0.14 and 0.18 $mM^{-1}s^{-1}$, respectively. In addition, **Oxo-TEMPO** showed no inflection point from 10 – 0.1 mM and an r_1 value of 0.15 $mM^{-1}s^{-1}$, suggesting that above CAC **TEMPO-UBD** exhibited a 1.2 times larger value than below CAC and **Oxo-TEMPO**, respectively. This result indicates that nano-particles exhibited larger r_1 values due to the suppression of fast molecular motion, as expected. Similarly, at pH 7.0 and 5.0, inflection concentration of r_1 value was observed and was consistent with the value obtained from τ_R. The resulting r_1 values below and above CAC were 0.17 and 0.21 $mM^{-1}s^{-1}$ at pH 7.0, and 0.15 and 0.19 $mM^{-1}s^{-1}$ at pH 5.0, respectively. In the r_2 values estimated from T_2-weighted images, r_2 values above CAC were 0.28, 0.33, and 0.39 $mM^{-1}s^{-1}$, at pH 5.0, 7.0, and 9.0, respectively, suggesting a strong pH dependency. The reference of **Oxo-TEMPO** showed a smaller value

of 0.19 $mM^{-1}s^{-1}$. As pH increased, the r_2 value increased in the order pH 9.0 > 7.0 > 5.0 and the resulting r_2 values were larger than that of the reference. Since the r_2 value is directly affected by the spin quantum number and the amount of spin number compared to r_1, the aggregate number of nano-particles at pH 9.0 might be the largest, and in the order pH 9.0 > 7.0 > 5.0. Plots of T_1^{-1} and T_2^{-1} *vs* concentration for **TEMPO-UBD** with **Oxo-TEMPO** at pH 9.0, 7.0, and 5.0 are shown in Figure 9, Figure S27(a) and (b) in S20. T_1- and T_2-weighted images at pH 7.0 are shown in Figure 10. The values of r_1 and r_2 at pH 9.0, 7.0, and 5.0 are summarized in Table 5.

(a) (b)

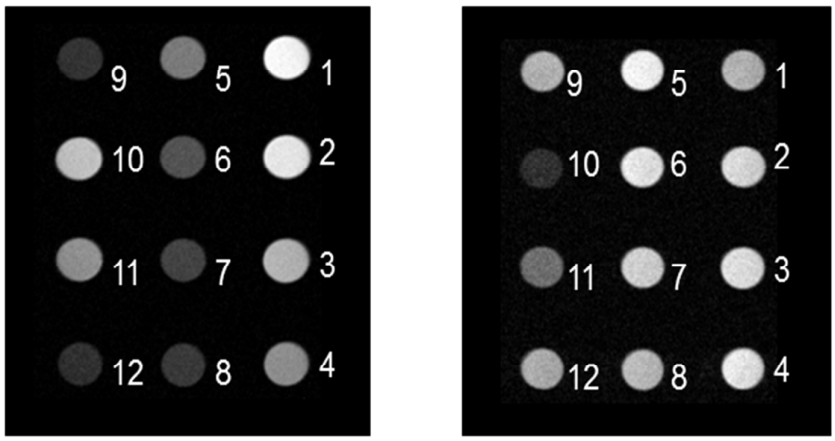

Figure 10. (a)T_1- and (b)T_2-weighted images of **TEMPO-UBD** at pH 7.0 and at various concentrations with standard materials. The numbers next to each image indicate the samples for 1) 10.0, 2) 7.5, 3) 5.0, 4) 3.3, 5) 2.5, 6) 1.0, 7) 0.5, 8) 0.25, and 9) 0.125 mM of **TEMPO-UBD**. 10) 0.25, 11) 0.125 mM of $MnCl_2$. 12) pure water, respectively.

Table 5. Values of r_1 and r_2 for **TEMPO-UBD** in Buffer Solutions under Various Conditions and a Blood Solution at pH 7.0 with Results of **Oxo-TEMPO** as Reference.

pH	**TEMPO-UBD**	
	r_1 ($mM^{-1}s^{-1}$)	r_2 ($mM^{-1}s^{-1}$)

9.0	Above CAC	0.18	0.39
	Below CAC	0.14	0.21
7.0	Above CAC	0.21	0.33
		0.24*	0.56*
		0.24#	0.38#
	Below CAC	0.17	N. D.
		0.20*	0.88*
		0.17#	0.25#
5.0	Above CAC	0.19	0.28
	Below CAC	0.15	0.22
		Oxo-TEMPO	
		0.15	0.19

* measured under blood solution. # after annealed at 70 ºC and measured 25 ºC.

Comparing the r_1 values above CAC at various pHs, the highest value was obtained in the neutral condition at pH 7.0 in spite of the highest τ_R value being seen at pH 9.0. This discrepancy between r_1 and τ_R values can be explained as follows. In the acidic condition at pH 5.0, the nano-particles showed smaller τ_R values in ESR because the nano-particles were carrying a cationic moiety, to lead a fast local motion of TEMPO moiety and/or fast global motion of the nano-particles due to Coulomb repulsion. While in the basic condition at pH 9.0, even though the nano-particles showed a larger τ_R value in ESR, the number of water molecules surrounding the TEMPO moiety is smaller owing to deprotonated tertiary N atoms and stronger hydrophobicity in the molecule. In the neutral condition at pH 7.0, even though the nano-particle showed a smaller τ_R value rather than those at pH 9.0, many water molecules exist surrounding TEMPO moiety so the largest r_1 values were observed due to

optimized conditions. Plausible molecular motions and environments of water molecules in nano-particles comprising **TEMPO-UBD** at pH 9.0, 7.0, and 5.0 are shown in Figure 11.

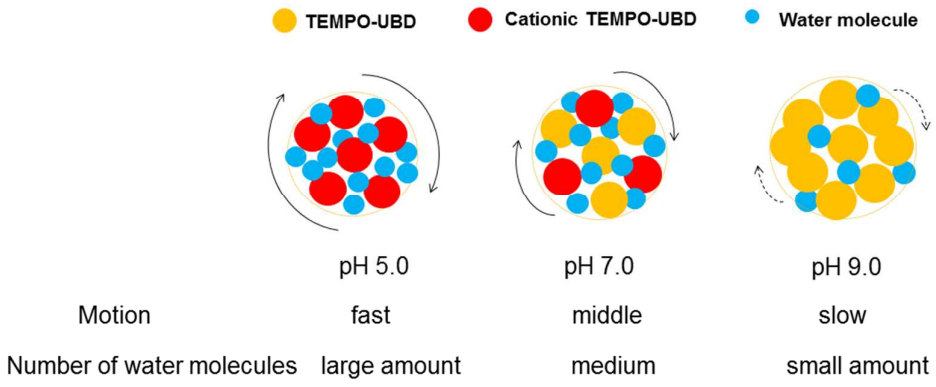

Figure 11. Schematic drawing of plausible molecular motions and environments of water molecules in nano-particles comprising **TEMO-UBD** at pH 9.0, 7.0, and 5.0.

For bio-imaging, furthermore, the stability of **TEMPO-UBD** in blood was confirmed by the variation of values of relaxivities (r_1 and r_2). The resulting values of r_1 and r_2 were 1.2 and 1.8 times larger than those in buffer solution at pH 7.0, suggesting that **TEMPO-UBD** was not labile in the blood and showed resistance against reductants such as ascorbic acid[27] and glutathione[28]. in blood. The reason for the increase of relaxivities might be the interaction between proteins such as albumin and increase size.[29] Surprisingly, increased values of r_1 and r_2 were also observed even with annealing treatment of the sample until 70 ºC. This result suggested that the heating process creates on the optimized formation of nano-particles for the increase of relaxivities and/or the water molecules re-oriented into **TEMPO-UBD**. Plots of T_1^{-1} and T_2^{-1} *vs* concentration for **TEMPO-UBD** in blood in Figure S28 in S21 and values are summarized in Table 5.

CONCLUSION.

In conclusion, we prepared a supra-molecular organic radical, **TEMPO-UBD**, carrying TEMPO radical as a candidate metal-free MRI contrast agent. **TEMPO-UBD** showed thermal and pH responsiveness in addition to MR function. In buffer solutions above CAC, **TEMPO-UBD** formed spherical nano-particle 20 - 150 nm in size. These nano-particles exhibited a two steps "double-LCST" thermos-responsive behavior and turned into micro-particles above LCST. This double-LCST is the first example among supra-molecules. As pH decreased, LCST values increased due to the formation of cationic **TEMPO-UBD**. To evaluate its potential as an MRI contrast agent, water-proton relaxivites, r_1 and r_2 were estimated under various pH conditions. The resulting r_1 and r_2 at pH 7.0 were 1.2 and 3 times larger than those of **Oxo-TEMPO**, indicating that an effective molecular size effect took place. In a blood sample, the relaxivities of r_1 and r_2 were 1.2 and 1.8 times larger than those in buffer solutions, indicating that **TEMPO-UBD** is not labile in a blood and thus is useful for bio-imaging. *In vivo* imaging using **TEMPO-UBD** is under investigation. In the present stage, no extremely large r_1 and r_2 values such as the nano-particles consisted of oligonucleotide-TEMPO system[9)] were observed. Because two insufficient factors to increase the r_1 and r_2 values were raised in the **TEMPO-UBD**. One is insufficient suppression of tumbling of the TEMPO moiety, another one is few number of water molecular surrounding the TEMPO. To prepare candidate MRI contrast agents having larger r_1 and r_2 values using the nano-particles, thus, the design and preparation of radicals introducing the polar moiety such as OEGs, hydroxyl and carboxylic acid neighboring the radical center are in progress.

EXPERIMENTAL SECTION.

General Information

Infrared and UV-Vis spectra were recorded. ^{1}H and ^{13}CNMR spectra were measured using $CDCl_3$ or DMSO-*d*6, or D_2O including TMS or DDS as standard material. HRMS using ESI mass spectra (ESI MS) were recorded. ESR spectra were recorded on X-band (9.4 GHz)

spectrometer equipped with a microwave frequency counter. Sample solutions in phosphate buffer were placed in capillary tubes and were measured at 25 °C. DLS measurements were performed. The images of transmission electron microscopy (TEM) images were obtained. The sample mounted on a carbon grid with hydrophilic treatment was stained with 5% uranyl acetate aq.. Scanning electron microscopy (SEM) was carried out. The samples were coated by Pt moisture by an ion coater and immobilized on a carbon tape onto a stage.

Relaxivity Measurements

The longitudinal (spin-lattice) and transverse (spin-spin) relaxation times (T_1 and T_2, respectively) were obtained on 25 MHz (0.59 T). The sample solutions (ca. 0.1 − 0.7 mM) in phosphate buffer were placed in 10 mm o.d. glass tubes and were measured at 25 °C. The values of relaxivity, r_1 and r_2, were calculated with equations (1) and (2).

$$1/T_1 = 1/T_0 + r_1C \quad (1)$$

$$1/T_2 = 1/T_0 + r_2C \quad (2)$$

, where T_0 and C are the relaxation time in the absence of the paramagnetic species and the concentration of the paramagnetic species, respectively.

***T_1*- and *T_2*-weighted MRI for samples.** MRI acquisitions of contrast agents were performed on a 7.0 T-MRI scanner with a volume coil (35 mm inner-diameter, transmission and reception). Aqueous solution of contrast agents (150 μl) was put into a polymerization chain reaction (PCR) tube cluster plate. The PCR tube cluster plate was set in the center of the volume coil. Sample temperature was maintained at 23.0 ± 0.5 °C throughout all experiments using a gradient coil cooling system and air conditioners. MRI scanner, horizontal single-slice T_1-weighted MR images were acquired with the following parameters: spin echo, TR/TE =400/9.6 ms, slice thickness = 2.0 mm, matrix = 256 × 256, field of view (FOV) =38.4 × 38.4 mm^2, number of averages (NA) = 1, number of slices = 1. For longitudinal relaxation time (T_1) and longitudinal relaxivity (r_1) calculations, horizontal single-slice inversion-recovery MRI was obtained using RARE (rapid acquisition with relaxation enhancement) acquisition

with the following parameters: TR = 10,000 ms, TE = 20 ms, inversion time = 52, 100, 200, 400, 800, 1600, 3200, 6400 ms, matrix size = 128 × 128, FOV = 38.4 × 38.4mm^2, slice thickness = 2.0 mm, RARE factor = 4, and NA = 1.

Materials Unless otherwise stated, the solvent and reagents were used without the purification. 2-Aminoethanol, 1,6-dibromohexane, 5-amino-1,3-isophthalicacid, potassium phthalimide, isophthaloyl chloride, and **Oxo-TEMPO** were purchased and used without purification. 2-(2-(2-methoxyethoxy)ethoxy)ethyl 4-methylbenzenesulfonate **(Eg_3Ts)** and tetramethyl-4-(4,4,5,5-tetramethyl-1,3,2-dioxaborolan-2-yl)-3,6-dihydropyridin-1(2*H*)-yloxyl radical were prepared according to the literatures.[14, 16] TLC was performed on silica gel plates 60 F_{254} (Merck).

11-(2-(2-(2-methoxyethoxy)ethoxy)ethyl)-2,5,8-trioxa-11-azatridecan-13-ol (**TEG_2EA**). To a solution of **Eg_3Ts** 33 g (0.10 mol) and 2-aminoethanol (2.5 g, 40 mmol) in 50 mL $CHCN_3$ was added K_2CO_3 (25g, 0.18 mol) and refluxed for 6 h. The solution was cooled to r.t. and the residual was removed by suction. The resulting solution was evaporated under reduced pressure. The crude residual was chromatographed on silica gel using with $CHCl_3$: MeOH (100 : 1 – 50 : 1) as eluent to afford a colorless oil (10.8g, 30.6 mmol) in 75% yield. IR (NaCl, cm^{-1}) 3472, 2873, 1456, 1352, 1294, 1245, 1200, 1108, 1045; ^{1}H-NMR ($CDCl_3$, 500 MHz) δ 3.67-3.60 (*m*, 12H), 3.59-3.51 (*m*, 10H), 3.38 (*s*, 6H), 2.79 (*t*, *J* = 5.7 Hz, 4H), 2.72 (*t*, *J* = 5.0 Hz, 2H); ^{13}C-NMR ($CDCl_3$) δ 71.9, 70.6, 70.5, 70.4, 69.8, 59.5, 59.0, 56.8, 54.2; ESI-MS m/z 354.25 $[M+H]^+$; HRMS (ESI) Calcd for $C_{16}H_{36}NO_7$ $[M+H]^+$: 354.2486, Found: 354.2519.

2-((6-bromohexyl)oxy)-N,N-bis(2-(2-(2-methoxyethoxy)ethoxy)ethyl)ethan-1-amine (**$Eg_3NEg_3C_6Br$**). To a solution of 1,6-dibromohexane (14.5 g, 59.4 mmol) in dist. THF (25 mL) was added a solution of NaH (1.5 g, 64 mmol) in dist. THF in an ice bath and stirred for several minutes. To the solution was added dropwise **TEG_2EA** (7.3 g, 21 mmol) in dist. THF (10 mL) and stirred overnight. To the reaction mixture was added *sat*. NH_4Cl aqueous and the mixture was extracted with Et_2O three times. The combined organic layer was dried over

$MgSO_4$, evaporated under reduced pressure, and the crude residual was chromatographed on silica gel using a mixture of $CHCl_3$: MeOH (100 : 1 – 50 : 1) as the eluent to afford a colorless oil (7.22 g, 14.0 mmol) in 68% yield. IR (NaCl, cm^{-1}) 2932, 2864, 1457, 1352, 1300, 1245, 1199, 1114, 1029; ^{1}H-NMR ($CDCl_3$, 500 MHz) δ 3.66-3.63 (*m*, 8H), 3.62-3.59 (*m*, 4H), 3.56-3.52 (*m*, 8H), 3.48 (*t*, *J* = 6.2 Hz, 2H), 3.42-3.39 (*m*, 4H), 3.38 (*s*, 6H), 2.80-2.75 (*m*, 6H), 1.86 (*quin*, *J* = 7.1 Hz, 2H), 1.57 (*quin*, *J* = 7.0 Hz, 2H), 1.45 (*quin*, *J* = 6.9 Hz, 2H), 1.36 (*quin*, *J* = 6.9 Hz, 2H); ^{13}C-NMR ($CDCl_3$) δ 72.0, 71.0, 70.6, 70.6, 70.4, 69.8, 69.4, 59.1, 54.7, 54.6, 33.9, 32.7, 29.5, 28.0, 25.4; ESI-MS m/z 538.23 $[M+Na]^+$; HRMS (ESI) Calcd for $C_{22}H_{46}BrNNaO_7$ $[M+Na]^+$: 538.2350, Found: 538.2317.

2-(11-(2-(2-(2-methoxyet)hoxy)ethoxy)ethyl)-2,5,8,14-tetraoxa-11-azaicosan-20-yl)isoindoline-1,3-dione (**$Eg_3NEg_3C_6Pht$**). A solution of **$Eg_3NEg_3C_6Br$** (7.22 g, 14.0 mmol) and potassium phthalimide (3.9 g, 21 mmol) in DMF (60 mL) was stirred at 110ºC for 4 h. To the reaction mixture was added water and extracted with Et_2O three times. The combined organic layer was dried over $MgSO_4$ and evaporated under reduced pressure. The crude residual was chromatographed on silica gel using $CHCl_3$: MeOH (100 : 1 – 50 : 1) as the elute to afford a colorless oil (6.48 g, 11.1 mmol) in 80% yield. IR (NaCl, cm^{-1}) 2932, 2863, 1772, 1714, 1467, 1436, 1396, 1369, 1301, 1249, 1199, 1113; ^{1}H-NMR ($CDCl_3$, 500 MHz) δ 7.84 (*d*, *J* = 5.4 Hz, 2H), 7.71(*d*, *J* = 5.4 Hz, 2H), 3.68 (*t*, *J* = 7.3 Hz, 2H), 3.65-3.59 (*m*, 12H), 3.56-3.53 (*m*, 8H), 3.40-3.38 (*m*, 8H), 2.80-2.74 (*m*, 6H), 1.68 (*quin*, *J* = 6.8 Hz, 2H), 1.55 (*quin*, *J* = 6.6 Hz, 2H), 1.47-1.35 (*m*, 4H); ^{13}C-NMR ($CDCl_3$, 126 MHz) δ 168.4, 133.9, 132.2, 123.2, 72.0, 71.1, 70.6, 70.6, 70.4, 69.8, 69.4, 59.0, 54.7, 54.6, 38.0, 29.6, 28.6, 26.7, 25.8; ESI-MS m/z 605.34 $[M+Na]^+$; HRMS (ESI) Calcd for $C_{30}H_{50}N_2NaO_9$ $[M+Na]^+$: 605.3409, Found: 605.3377.

6-((11-(2-(2-(2-methoxyethoxy)ethoxy)ethyl)-2,5,8-trioxa-11-azatridecan-13-yl)oxy)hexan-1-amine (**$Eg_3NEg_3C_6NH_2$**). To a solution of **$Eg_3NEg_3C_6Pht$** (6.5 g, 11 mmol) in EtOH (130 mL) was added dropwise hydrazine monohydrate (2.2 g, 44 mmol) and refluxed for 4 h. The reaction mixture was evaporated under reduced pressure and the crude residual was diffused

with Et_2O. The insoluble mixture in Et_2O was removed by suction filtration and the filtrate was evaporated. The crude residual was chromatographed on silica gel using $CHCl_3$: MeOH (100 : 1 - 50 : 1 with 5% trimethylamine) to afford a colorless oil (3.92 g, 8.65 mmol) in 78% yield. IR (NaCl, cm^{-1}) 3371, 2929, 2862, 1577, 1458, 1351, 1328, 1303, 1249, 1199, 1113; ^{1}H-NMR ($CDCl_3$, 500 MHz) δ 3.65-3.62 (*m*, 8H), 3.61-3.59 (*m*, 4H), 3.56-3.52 (*m*, 8H), 3.48 (*t*, *J* = 6.2 Hz, 2H), 3.40 (*t*, *J* = 6.7 Hz, 2H), 3.38 (*s*, 6H), 2.80-2.75 (*m*, 6H), 2.68 (*t*, *J* = 7.0 Hz, 2H), 1.56 (*quin*, *J* = 6.6 Hz, 2H), 1.44 (*quin*, *J* = 6.7 Hz, 2H), 1.38-1.30 (*m*, 4H); ^{13}C-NMR ($CDCl_3$, 126 MHz) δ 72.0, 71.2, 70.7, 70.6, 70.4, 69.8, 69.4, 59.1, 54.7, 54.6, 42.2, 33.7, 29.7, 26.7, 26.1; ESI-MS m/z 453.35 $[M+H]^+$; HRMS (ESI) Calcd for $C_{22}H_{49}N_2O_7$ $[M+H]^+$: 453.3534, Found: 453.3505.

1,1'-(5-iodo-1,3-phenylene)bis(3-(11-(2-(2-(2-methoxyethoxy)ethoxy)ethyl)-2,5,8,14-tetraoxa-11-azaicosan-20-yl)urea) (**Iodo-UBD**). A solution of 5-iodoisophthalic acid (584 mg, 2 mmol) in $SOCl_2$ (30 mL) was refluxed for 2h and evaporated under reduced pressure, to afford a crude 5-iodoisophthaloylchloride. To a solution of the crude mixture in THF (4 mL) was added NaN_3 (860 mg, 13 mmol) in a water solution and stirred in an ice bath for 2h. To the mixed solution was added sat. $NaHCO_3$ solution and extracted with toluene three times. The combined organic layer was dried over $MgSO_4$ and evaporated under reduced pressure until 15 mL, to afford a toluene solution of 5-iodoisophthaloyl diazide. Without purification, the crude reaction mixture was refluxed for 2 h, to afford a toluene solution including 1-iodo-3,5-diisocyanatobenzene. To a solution of 1-iodo-3,5-diisocyanatobenzene in toluene was added dropwise of $\mathbf{Eg_3NEg_3C_6NH_2}$ (2.0 g, 4.4 mmol) in 8 mL CH_2Cl_2 in an ice bath, and stirred overnight at r.t.. The reaction mixture was evaporated under reduced pressure, and the crude residual was chromatographed on silica gel using $CHCl_3$: MeOH (100 : 1 – 50 : 1) as eluent to afford a yellowish oil (1.45 g, 1.22 mmol) in 61%. The reactions of 5-iodoisophthaloyl dichloride, 5-iodoisophthaloyl diazide, and 1-iodo-3,5-diisocyanatobenzene were monitored by IR spectra, respectively. IR (NaCl, cm^{-1})

3491, 3340, 2930, 2864, 1695, 1594, 1538, 1449, 1351, 1305, 1261, 1201, 1111 1028; ^{1}H-NMR (DMSO-*d*6, 500 MHz) *δ* 8.44 (*s*, 2H), 7.45 (*d*, *J* = 1.8 Hz, 2H), 7.28 (*t*, *J* = 1.8 Hz, 1H), 6.06 (*t*, *J* = 5.6 Hz, 2H), 3.51-3.46 (*m*, 24H), 3.44-3.41 (*m*, 16H), 3.40-3.35 (*m*, 8H), 3.23 (*s*, 12H), 3.04 (*q*, *J* = 6.4 Hz, 4H), 2.65 (*t*, *J* = 6.2 Hz, 12H), 1.48 (*quin*, *J* = 6.7 Hz, 4H), 1.41 (*quin*, *J* = 6.7 Hz, 4H), 1.32-1.26 (*m*, 8H), ^{13}C-NMR (DMSO-*d*6, 126 MHz) δ 155.3, 142.6, 119.0, 106.1, 95.0, 79.6, 71.8, 70.6, 70.3, 70.2, 70.1, 69.7, 66.8, 58.5, 54.6, 30.1, 29.7, 26.7, 25.9, ESI-MS m/z 596.32 $[M+2H]^{2+}$, HRMS (ESI) Calcd for $C_{52}H_{101}N_6O_{16}I$ $[M+2H]^{2+}$: 596.3154, Found: 596.3154.

1,1'-(1,3-phenylene)bis(3-(11-(2-(2-(2-methoxyethoxy)ethoxy)ethyl)-2,5,8,14-tetraoxa-11-aza icosan-20-yl)urea) **(H-UBD)**. **H-UBD** was prepared in a manner similar to **Iodo-UBD** using isophthaloyl chloride in place of 5-iodoisophthaloyl chloride. A yellowish oil (1.6 g, 1.5 mmol) was obtained in 76% yield. IR (NaCl, cm^{-1}) 3502, 3346, 2931, 2863, 1689, 1606, 1549, 1482, 1455, 1421, 1351, 1302, 1238, 1201, 1110, 1028; ^{1}H-NMR (DMSO-*d*6, 500 MHz) δ 8.31 (*s*, 2H), 7.43 (*t*, *J* = 1.8 Hz, 1H), 7.01 (*t*, *J* = 8.0 Hz, 1H), 6.93 (*dd*, *J* = 1.8 Hz, 8.0 Hz, 2H), 6.00 (*t*, *J* = 5.6 Hz, 2H), 3.48-3.51 (*m*, 24H), 3.38-3.44 (*m*, 20H), 3.32-3.36 (*m*, 4H), 3.23 (*s*, 12H), 3.05 (*q*, *J* = 6.5 Hz, 4H), 2.65 (*t*, *J* = 6.1 Hz, 12H), 1.48 (*quin*, *J* = 6.7 Hz, 4H), 1.40 (*quin*, *J* =6.7 Hz, 4H), 1.33-1.29 (*m*, 8H); ^{13}C-NMR ($CDCl_3$, 126 MHz) δ 155.6, 141.4, 129.2, 110.8, 107.2, 79.7, 71.8, 70.6, 70.3, 70.2, 70.1, 69.7, 69.5, 58.5, 54.6, 30.2, 29.7, 26.7, 26.0; ESI-MS m/z 533.37 $[M+2H]^{2+}$; HRMS (ESI) Calcd for $C_{52}H_{102}N_6O_{16}$ $[M+2H]^{2+}$: 533.3671, Found: 533.3696.

1,1'-(5-(1-oyl-2,2,6,6-tetramethyl-3-dihydropyridin-4-yl)benzene-1,3-diyl)bis(3-(11-(2-(2-(2-methoxyethoxy)ethoxy)ethyl)-2,5,8,14-tetraoxa-11-azaicosan-20-yl)urea) (**TEMPO-UBD**). **Iodo-UBD** (596 mg, 0.5 mmol), $Pd(PPh_3)_4$ (28.9 mg, 0.025 mmol), 2,2,6,6-tetramethyl-4-(4,4,5,5-tetramethyl-1,3,2-dioxaborolan-2-yl)-3,6-dihydropyridin-1(2*H*) -yloxyl Radical (168 mg, 0.6 mmol), and degassed 1,4-dioxane (4 mL) were placed in a three neck flask and a bubbling treatment of the mixed solution using N_2 gas was carried out

carefully for 30 min. To the reaction mixture was added 10% Na_2CO_3 aq. and stirred at 100 °C for 6 h. The reaction mixture added with brine was extracted with $CHCl_3$ three times and the combined organic layer was dried over $MgSO_4$ and then evaporated under reduced pressure. The crude residual was chromatographed on silica gel using $CHCl_3$: MeOH (100 : 1 – 50 : 1) as elute to afford a brown wax-like solid (344 mg, 0.28 mmol) in 57% yield; IR (NaCl, cm^{-1}) 3516, 3339, 2929, 2862, 1696, 1668, 1602, 1558, 1453, 1360, 1249, 1201, 1114, 1033, 850; ^{1}H-NMR (DMSO-*d*6 + ascorbic acid, 500 MHz) δ 8.34 (*s*, 2H), 7.29 (*t*, *J* = 1.7 Hz, 1H), 7.04 (*d*, *J* = 1.7 Hz, 2H), 5.98 (*t*, *J* = 5.6 Hz, 2H), 5.78 (*s*, 1H), 3.52-3.47 (m, 44H), 3.36 (*t*, J = 6.4 Hz, 4H), 3.23 (*s*, 12H), 3.05 (*q*, *J* = 6.4 Hz, 4H), 2.30 (*s*, 2H), 1.49 (*quin*, *J* = 6.7 Hz, 4H), 1.41 (*quin*, *J* = 6.7 Hz, 4H), 1.33-1.27 (*m*, 8H), 1.20 (*s*, 6H), 1.12 (*s*, 6H); ^{13}C-NMR (DMSO-*d*6 + ascorbic acid, 126 MHz) δ 155.6, 141.6, 141.3, 131.8, 130.2, 107.8, 105.9, 91.8, 88.4, 73.7, 71.7, 70.7, 70.2, 70.0, 68.4, 58.5, 54.3, 30.2, 29.6, 26.7, 25.9, ESI-MS m/z 609.42 $[M+2H]^{2+}$; HRMS (ESI) Calcd for $C_{61}H_{116}N_7O_{17}$ $[M+2H]^{2+}$: 609.4208, Found: 609.4212.

ASSOCIATED CONTENT

Supporting Information

The Supporting Information is available free of charge on the ACS Publication website at DOI: 10.1021/acs.joc.

Copies of ^{1}H- and ^{13}C-NMR for new materials. Additional data of ^{1}H-NMR spectra for **H-UBD** and ESR spectra for **TEMPO-UBD** in various aqueous conditions. Additional plots of the transmittance at 800 nm vs temperature, number vs D_H, and relaxation rate vs concentration for **H-** and **TEMPO-UBD** in various conditions.

AUTHOR INFORMATION

Corresponding Author

E-mail: karasawa@phar.kyushu-u.ac.jp (S. K.).

Note

Authors declare no competing financial interests.

ACKNOWLEDGMENTS

The authors thank Ms. Sayaka Shibata, Mr. Nobuhiro Nitta and Yoshikazu Ozawa (National Institute of Radiological Sciences; NIRS, QST) for MRI operation. S. K. thanks Dr. Noboru Koga for many helpful discussions. This work was partially supported by Platform for Drug Discovery, Informatics, and Structural Life Science from the Ministry of Education, Culture, Sports, Science and Technology (MEXT), Japan, Grants-in-Aid for exploratory Research (No. 26620070) from the Japan Society for the Promotion of Science (JSPS), PRESTO program on Molecular Technology from Japan Science Technology Agency (JST). MR imaging and analysis are also financially supported by the Center of Innovation Program (COI) streams from JST and Jisedai/innovative cancer grants from Japan Agency for Medical Research and Development (AMED).

REFERENCES.

1. a) Laurent, S.; Forge, D.; Port, M.; Roch, A.; Robic, C.; Elst, L. V.; Muller, R. N. *Chem. Rev*. **2008**, *108*, 2064 – 2110. b) Hao, R.; Xing, R.; Xu, Z.; Hou, Y.; Gao, S.; Sun, S. *Adv. Mater*. **2010**, *22*, 2729 – 2742. c) Gale, E. M.; Atanasova, I. P.; Blasi, F.; Ay, I.; Caravan, P. *J. Am. Chem. Soc*. **2015**, *137*, 15548 – 15557.
2. a) Rocca, J. D.; Liu, D.; Lin, W. *Accounts Chem. Res*. **2011**, *44*, 957 – 968. b) Caravan, P.; Ellison, J. J.; McMury, T. J.; Lauffer, R. B. *Chem. Rev*. **1999**, *99*, 2293 – 2352.
3. a) Baranyai, Z.; Pálinkás, Z.; Uggeri, F.; Maiocchi, A.; Aime, S.; Brücher, E. *Chem. Eur. J.* **2012**, *18*, 16426 – 16435. b) Frenzel, T.; Lengsfeld, P.; Schirmer, H.; Hütter, J.; Weinmann, H. J. *Invest. Radiol*, **2008**, *43*, 817 – 828.
4. Kanda, T.; Ishii, K.; Kawaguchi, H.; Kitajima, K.; Takenaka, D. *Radiology*, **2014**, *270*, 834

– 841.

5. a) Yamada, KI.; Yamamiya, I, Utsumi, H. *Free Radic. Res.* **2006**, *40*, S151. b) Kuppusamy, P.; Ilangovan, G. H. L.; Cardounel, A. J.; Zweier, J. L.; Yamada, K.; Krishna, M. C.; Mitchell, J. B. *Cancer Res.* **2002**, 62, 307 – 312.

6. a) Yamato, M.; Kudo, W.; Shiba, T.; Yamada, KI, Watanabe, T.; Utumi, H. *Free Radic. Res*. **2010**, *44*, 249 – 257. b) Zhang, R. L.; Goldstein, S.; Samuni, A. *Free Radic. Biol. Med*. **1999**, *26*, 1245 – 1252.

7. a) Cheng, Z.; Thorek, D. L. J.; Tsourkas, A. *Adv. Funct. Mater*. **2009**, *19*, 3753 – 3759. b) Winalski, C. S.; Shorkroff, C. S.; Mulkern, R. V.; Schneider, E.; Rosen, G. M. *Magn. Reson. Med*. **2002**, *48*, 965 – 972. c) Li, Y.; Lei, X.; Lawler, R. G.; Murata, Y.; Komatsu, K.; Turro, N. J. *J. Phys. Chem. Lett.* **2010**, *1*, 2135 – 2138.

8. a) Rajca, A.; Wang, Y.; Boska, M.; Paletta, J. T.; Olankitwanit, A.; Swanson, M. A.; Mitchell, D. G.; Eaton, S. S.; Eaton, G. R. Rajca, S. *J. Am. Chem. Soc*. **2012**, *134*, 15724 – 15727. b) Hayashi, H.; Karasawa, S.; Tanala, A.; Odoi, K.; Chikama, K.; Kuribayashi, H.; Koga, N. *Mag. Reson. Chem,* **2009**, *47*, 201−204. c) Hayashi, H,; Karasawa, S.; Koga, N. *J. Org. Chem*. **2008**, *73*, 8683 – 8693.

9. Tanimoto, E.; Karasawa, S.; Ueki, S.; Nitta, N.; Aoki, I.; Koga, N. *RSC Adv.*, **2013**, *3*, 3531−3534.

10. a) Sato, Y.; Hayashi, H.; Okazaki, M.; Aso, M.; Karasawa, S.; Ueki, S.; Suemune, H.; Koga, N. *Mag. Reson. Chem.,* **2008**, *46*, 1055−1058. b) Okazaki, M.; Sato, Y.; Karasawa, S.; Koga, N. *Nucle, Acid, Symp, Ser*, **2008**, 52, 375−376.

11. Hayashi, H.; Ohkubo, K.; Karasawa, S.; Koga, N. *Langmuir,* **2011**, *27*, 12709−12719.

12. Tachaboonyakiat, W.; Ajiro, H.; Akashi, M. *Polymer Journal*, **2013**, *45*, 971 – 978.

13. a) Betancourt, J. E.; Rivera, J. M. *Langmuir*, **2015**, *31*, 2095 – 2103. b) Arai, M.; Ito, K. *Chem. Lett*. **2015**, *44*, 1416 – 1418. c) Harada, A.; Takashima, Y.; Nakahata, M. *Acc. Chem. Res*. **2014**, *47*, 2128 – 2140. d) Liong, M.; Lu, Jie, Kovochich, M.; Xia, T.; Ruehm, S. G.;

Nel, A. E.; Tamanoi, F.; Zink, J. I. *ACS Nano*, **2008**, *2*, 889 – 896.

14. Manfredi, N.; Cecconi, B.; Calabrese, V.; Minotti, A.; Peri, F.; Ruffo, R.; Monai, M.; Romero-Ocaña, Montini, T.; Fornasiero, P.; Abbotto, A. *Chem. Commun*. **2016**, *52*, 6977 – 6980.

15. a) Iwanaga, T.; Ogawa, M.; Yamauchi, T.; Toyota, S. *J. Org. Chem.* **2016**, *81*, 4076 – 4080. b) Raders, S. M.; Moore, J. N.; Parks, J. K.; Miller, A. D.; Leißing, T. M.; Kelley, S. P.; Rogers, R. D.; Shaughnessy, K. H. *J. Org. Chem.* **2013**, *78*, 4649 – 4664.

16. Kálai, T.; Jekö, J.; Berente, Z.; Hideg, K. *Synthesis*, **2006**, *3*, 439 – 446.

17. Tataurova, Y.; Sealy, M. J.; Larsen, R. G.; Larsen, S. C. *J. Phys. Chem. Lett.* **2012**, *3*, 425-429.

18. Kakehashi, R.; Shizuma, M.; Yamamura, S.; Maeda, H. *J. Colloid. Interface Sci*. **2005**, *289*, 498 – 503.

19. a) Li, Z.; Chen, C.; Gröger, S.; Kressler, J. *Polymer*, **2012**, *53*, 2613 – 2618. b) Seco, J. M.; Latypov, S. K.; Quiñoá, E.; Riguera, R. *J. Org. Chem*. **1997**, *62*, 7569 – 7574.

20. a) Fielding, L. A.; Lane, J. A.; Derry, M. J.; Mykhaylyk, O. O.; Armes, S. P. *J. Am. Chem. Soc*. **2014**, *136*, 5790-5798. b) Hosono, N.; Gillissen, M. A. J.; Li, Y.; Sheiko, S. S.; Palmans, A. R. A.; Meijer, E. W. *J. Am. Chem. Soc*. **2013**, *135*, 501-510.

21. Mousseau, J. J.; Xing, L.; Tang, N.; Cuccia, L. A. *Chem. Eur. J*. **2009**, *15*, 10030 – 10038.

22. Ponnuswamy N.; Pantoş G. D.; Smulders M. M. J.; Sanders, J. K. M. *J. Am. Chem. Soc*. **2012**, *134*, 566-573.

23. de Greef, T. F. A.; Smulders, M. M. J.; Wolffs, M.; Schenning, A. P. J.; Sijbesma, R. P.; Meijer E. W. *Chem. Rev.* **2009**, *109*, 5687 – 5754.

24. a) Kundu, K.; Das, R. *Mole. Phys*. **2014**, *112*, 1577 – 1588. b) Kivelson D. *J. Chem. Phys*. **1966**, *45*, 1324.

25. a) Liang, X.; Kozlovskaya, V.; Palchak, Z.; Kharlampieva, E. *ACS Macro Lett*. **2015**, 4, 308 – 311. b) Chen, X. L.; Sun, H.; Xu, J.; Han, X.; Liu, H. L.; Hu, Y. *RSC Adv*. **2015**, *5*,

86584 – 86592.

26. Heyda, J.; Soll, S.; Yuan, J.; Dzubiella, J. *Macromolecules*, **2014**, *47*, 2096 – 2102.

27. a) Eggersdorfer, M.; Laudert, D.; Létinolis, U.; McClymont, T.; Medlock, J.; Netschere, T.; Bonrath, W. *Angew. Chem. Int. Ed*. **2012**, *51*, 12960 – 12990. b) Packer, J. E.; Slater, T. F.; Willson, R. L.; *Nature*, **1979**, *278*, 737 – 738.

28. a) Banhegyi, G.; Braun, L.; Csala, M.; Puskas, F. Free Radic. Biol. Med. **1997**, *23*, 793 – 803. b) Braun, L.; Puskas, F.; Csala, M.; Meszaros, G.; Mandl, J.; Banhegyi, G. Free Radic. Biol. Med. **1997**, *23*, 804 – 808. c) Basu, S.; Som, S.; Deb, S.; Mukherjee, D.; Chatterjee, I. B. *Biochem. Bioph. Res. Commun*. **1979**, *90*, 1335 – 1340.

29. Goswami, L. N.; Cai, Q.; Ma, L.; Jalisatgi, S. S.; Hawthorne, M. F. *Org. Biomol. Chem*. **2015**, *13*, 8912 – 8918.

TOC

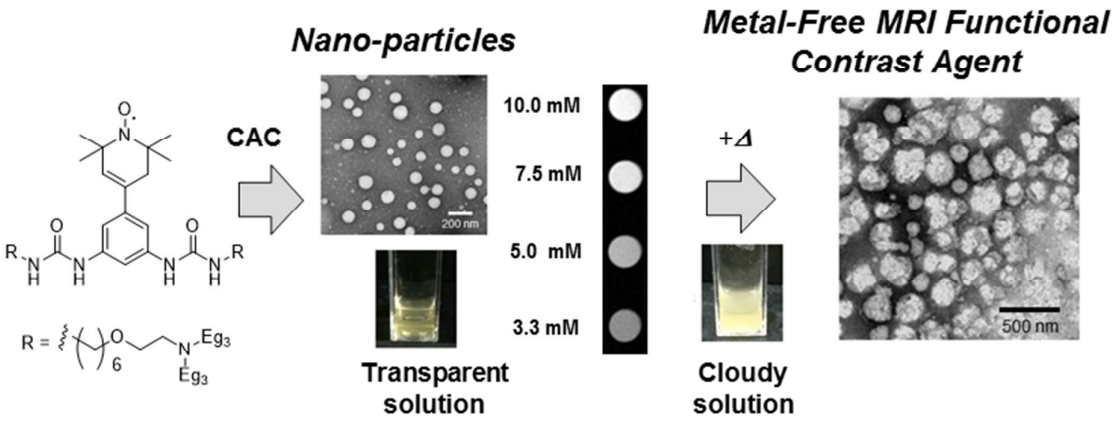
Nano-particles
Metal-Free MRI Functional Contrast Agent
CAC
+Δ
10.0 mM
7.5 mM
5.0 mM
3.3 mM
200 nm
500 nm
Transparent solution
Cloudy solution